Asymmetric Cooperative Catalysis of Strong Brønsted Acid Promoted Reactions Using Chiral Ureas

Hao Xu, *et al.*

Science **327**, 986 (2010);
DOI: 10.1126/science.1182826

silicate minerals and hence readily available silicate ions.

References and Notes

1. A. Butlerow, *Justus Liebigs Ann. Chem.* **120**, 295 (1861).
2. O. Loew, *J. Prakt. Chem.* **34**, 51 (1886).
3. N. W. Gabel, C. Ponnamperuma, *Nature* **216**, 453 (1967).
4. L. E. Orgel, *Crit. Rev. Biochem. Mol. Biol.* **39**, 99 (2004).
5. R. Breslow, *J. Am. Chem. Soc.* **80**, 3719 (1958).
6. T. Matsumoto, S. Inoue, *J. Chem. Soc. Perkin Trans. I* **1982**, 1975 (1982).
7. A. W. Schwartz, R. M. de Graaf, *J. Mol. Evol.* **36**, 101 (1993).
8. A. G. Cairns-Smith, P. Ingram, G. L. Walker, *Theor. Biol.* **35**, 601 (1972).
9. L. E. Orgel, *Proc. Natl. Acad. Sci. U.S.A.* **97**, 12503 (2000).
10. R. Krishnamurthy, S. Pitsch, G. Arrhenius, *Orig. Life Evol. Biosph.* **29**, 139 (1999).
11. S. Pitsch, R. Krishnamurthy, G. Arrhenius, *Helv. Chim. Acta* **83**, 2398 (2000).
12. Materials and methods are available as supporting material on *Science* Online.
13. R. Breslow, *Tetrahedron Lett.* **1**, 22 (1959).
14. R. F. Socha, A. H. Weiss, M. M. Sakharov, *J. Catal.* **67**, 207 (1981).
15. G. O. Arrhenius, *Helv. Chim. Acta* **86**, 1569 (2003).
16. R. Shapiro, *Orig. Life Evol. Biosph.* **18**, 71 (1988).
17. P. Decker, H. Schweer, R. Pohlmann, *J. Chromatogr. A* **244**, 281 (1982).
18. V. M. Kolb, J. P. Dworkin, S. L. Miller, *J. Mol. Evol.* **38**, 549 (1994).
19. R. Larralde, M. P. Robertson, S. L. Miller, *Proc. Natl. Acad. Sci. U.S.A.* **92**, 8158 (1995).
20. Y. Shigemasa, S. I. Akagi, E. Waki, R. Nakashima, *J. Catal.* **69**, 58 (1981).
21. Y. Shigemasa *et al.*, *Carbo. Res.* **134**, C4 (1984).
22. G. Springsteen, G. F. Joyce, *J. Am. Chem. Soc.* **126**, 9578 (2004).
23. A. Ricardo, M. A. Carrigan, A. N. Olcott, S. A. Benner, *Science* **303**, 196 (2004).
24. A. N. Simonov *et al.*, *Adv. Space Res.* **40**, 1634 (2007).
25. D. S. Kelley *et al.*, *Science* **307**, 1428 (2005).
26. N. G. Holm, M. Dumont, M. Ivarsson, C. Konn, *Geochem. Trans.* **7**, 7 (2006).
27. W. Stumm, J. J. Morgan, *Aquatic Chemistry* (Wiley-Interscience, New York, ed. 3, 1996).
28. J. Washington, *Orig. Life Evol. Biosph.* **30**, 53 (2000).
29. R. M. Hazen, D. S. Sholl, *Nat. Mater.* **2**, 367 (2003).
30. S. D. Kinrade, R. J. Hamilton, A. S. Schach, C. T. B. Knight, *J. Chem. Soc., Dalton Trans.* (7) 961 (2001).
31. J. B. Lambert, G. Lu, S. R. Singer, V. M. Kolb, *J. Am. Chem. Soc.* **126**, 9611 (2004).
32. X. Kästele, P. Klüfers, F. Kopp, J. Schuhmacher, M. Vogt, *Chem. Eur. J.* **11**, 6326 (2005).
33. X. Yang, P. Roonasi, A. Holmgren, *J. Colloid Surf. Sci.* **328**, 41 (2008).
34. G. C. S. Collins, W. O. George, *J. Chem. Soc. B* **1971**, 1352 (1971).
35. M. Z. Iqbal, S. Novalin, *J. Chromatogr. A* **1216**, 5116 (2009).
36. F. García-Jiménez, O. Collera Zúñiga, Y. Castells García, J. Cárdenas, G. Cuevas, *J. Braz. Chem. Soc.* **16**, (3a), 467 (2005).
37. L. Que, G. R. Gray, *Biochem.* **13**, 146 (1974).

38. This research was supported by the National Science Foundation, Dow Corning Corp., and Schlumberger Ltd.

Supporting Online Material

www.sciencemag.org/cgi/content/full/327/5968/984/DC1
Materials and Methods
Figs. S1 to S13

30 September 2009; accepted 5 January 2010
10.1126/science.1182669

Asymmetric Cooperative Catalysis of Strong Brønsted Acid–Promoted Reactions Using Chiral Ureas

Hao Xu, Stephan J. Zuend, Matthew G. Woll, Ye Tao, Eric N. Jacobsen*

Cationic organic intermediates participate in a wide variety of useful synthetic transformations, but their high reactivity can render selectivity in competing pathways difficult to control. Here, we describe a strategy for inducing enantioselectivity in reactions of protio-iminium ions, wherein a chiral catalyst interacts with the highly reactive intermediate through a network of noncovalent interactions. This interaction leads to an attenuation of the reactivity of the iminium ion and allows high enantioselectivity in cycloadditions with electron-rich alkenes (the Povarov reaction). A detailed experimental and computational analysis of this catalyst system has revealed the precise nature of the catalyst-substrate interactions and the likely basis for enantioinduction.

The proton (H^+) is the simplest, and arguably the most versatile, catalyst for organic reactions, mediating an extraordinary range of biological and synthetic transformations (*1*). Although a proton cannot be rendered chiral, enantioselective Brønsted acid catalysis is attainable through the influence of the acid's conjugate base and through medium effects. The former strategy, involving the use of chiral acids, has proven particularly useful, as demonstrated in the design and application of chiral phosphoric acids (*2*–*4*), *N*-triflyl phosphoramides (*5*), aryl sulfonic acids (*6*), and Lewis acid– (*7*, *8*) or thiourea-assisted Brønsted acids (*9*, *10*). The use of medium effects has been less straightforward, and chiral solvents have been investigated in asymmetric catalysis with comparatively limited success (*11*). The recent discovery of anion-binding pathways (*12*, *13*) in reactions catalyzed by chiral, small-molecule, H-bond donor catalysts such as urea and thiourea derivatives (*14*) suggests an alternative strategy that combines elements of both approaches. In this scenario, a chiral catalyst might associate with a protonated substrate through the counteranion and induce enantioselectivity in nucleophilic addition reactions to the cationic electrophile through specific secondary interactions with the charged species.

This idea was explored in the context of the formal [4+2] cycloaddition of *N*-aryl imines and electron-rich olefins, also known as the Povarov reaction (*15*). This Brønsted acid–catalyzed reaction affords tetrahydroquinoline derivatives with the concomitant generation of up to three contiguous stereogenic centers, and enantioselective Lewis acid– or phosphoric acid–catalyzed variants have been identified recently (*16*–*18*). The acid-catalyzed Povarov reaction between benzylidene aniline **2a** and 2,3-dihydrofuran **3** was selected as a model reaction (Fig. 1A), and a broad range of chiral urea and thiourea derivatives that were developed and studied previously in our laboratory, as well as several different Brønsted acids, were evaluated as catalysts for this transformation (table S1) (*19*). With this approach, we found that the combination of the bifunctional sulfinamido urea derivative **1a** (*20*) and *ortho*-nitrobenzenesulfonic acid (NBSA) catalyzed the model reaction with high enantioselectivity (Fig. 1, B and C, entry 1). The importance of both the urea and sulfinamide groups in the catalyst became evident in structure-reactivity/enantioselectivity studies. Thiourea derivative **1b** is an efficient catalyst, but it induced lower enantio- and diastereoselectivity (Fig. 1C, entry 2), whereas the diastereoisomeric (*R*,*R*,*S*)-sulfinamido urea **1c** promoted a much slower and poorly selective reaction (Fig. 1C, entry 3). In addition, reactions catalyzed by phosphinic amide urea **1d** displayed a modest selectivity, and pivalamide urea **1e** and amino urea **1f** both induced low reactivity and selectivity (Fig. 1C, entries 4 to 6). These results suggest a cooperative role for the urea and sulfinamide groups of **1a** in the rate- and enantioselectivity-determining steps of the catalytic reaction.

Under optimized conditions, the Povarov reaction that is catalyzed by **1a** was found to be applicable to different nucleophiles and a wide variety of *N*-aryl imines (Fig. 2, A and B). The highest enantioselectivities were observed in reactions that were carried out under cryogenic conditions with a 2:1 ratio of **1a** to NBSA, which was used to ensure complete suppression of the racemic pathway catalyzed by NBSA alone. Lactam-substituted tetrahydroquinoline derivatives $\mathbf{6}_{\mathbf{exo}}$ were obtained in high enantio- and diastereoselectivities by reaction of benzaldimines **2** with vinyllactam **5**. Tricyclic hexahydropyrrolo-[3,2-*c*]quinoline derivatives $\mathbf{8}_{\mathbf{exo}}$ were generated in an analogous manner by the cyclization of *N*-Cbz–protected 2,3-dihydropyrrole **7** with **2**.

Department of Chemistry and Chemical Biology, Harvard University, Cambridge, MA 02138, USA.

*To whom correspondence should be addressed. E-mail: jacobsen@chemistry.harvard.edu

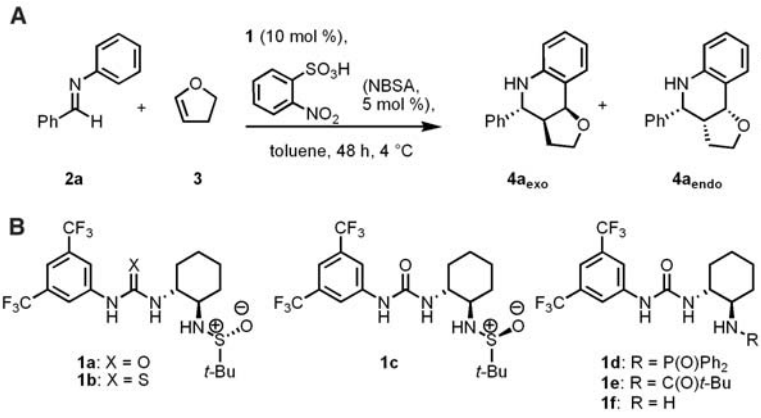

C

entry	catalyst	conversion (%)	dr ($4_{exo}/4_{endo}$)	4_{exo} ee (%)
1	**1a**	92	4.0	91
2	**1b**	95	1.4	83
3	**1c**	52	0.3	2
4	**1d**	20	1.0	50
5	**1e**	8	0.25	<5
6	**1f**	0	ND	ND

Fig. 1. (**A**) Model Povarov reaction cocatalyzed by *o*-nitrobenzenesulfonic acid and chiral ureas/thioureas. (**B**) Some of the chiral catalysts evaluated in optimization studies. (**C**) Results of catalyst structure-reactivity/enantioselectivity studies. dr, diastereomeric ratio;. Both dr and ee were determined by supercritical fluid chromatography analysis using commercially available chiral columns (*19*).

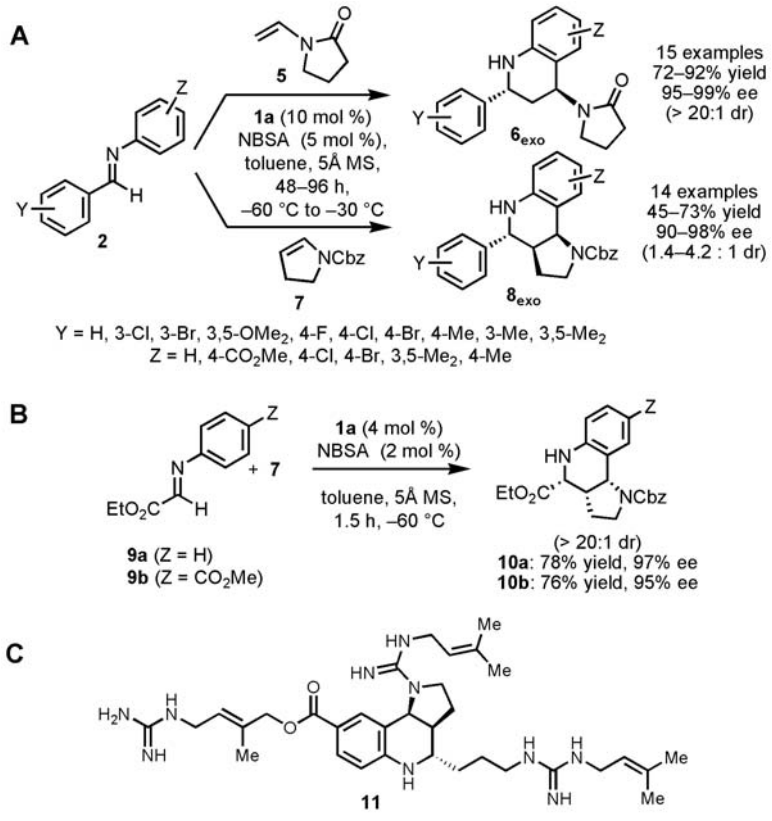

Fig. 2. (**A** and **B**) Asymmetric Povarov reactions catalyzed by **1a**/NBSA with enamide **5** and enecarbamate **7** as the nucleophilic reacting partners. Molecular sieves (5 Å) serve to sequester water introduced with the hygroscopic NBSA reagent, thereby preventing competing imine hydrolysis pathways. See tables S2 and S3 for yields and selectivities obtained with each substrate. (**C**) Martinelline (**11**), a natural-product inhibitor of bradykinin B1 and B2 G protein-coupled receptors (median inhibitory concentration IC_{50} = 6.4 and 0.25 μM, respectively). A previous study demonstrated that a racemic form of ester **10b** could be converted to (±)**11** after epimerization of the corresponding aldehyde, so the enantioselective synthesis of **10b** described here constitutes a formal enantioselective synthesis of martinelline (*25*).

Although moderate diastereoselectivities favoring the exo diastereomer were obtained in this case ($\mathbf{8}_{exo}/\mathbf{8}_{endo}$ = 1.4 to 4.2:1), this product was also generated in high enantiomeric excess (ee) (90 to 98% ee) and could be isolated in diastereomerically pure form in useful yields (45 to 73%). In general, imines derived from electron-deficient aldehydes—especially imines derived from glyoxylate esters—underwent reaction more rapidly in the Povarov reaction, but uniformly high enantioselectivities were obtained despite these reactivity differences.

Povarov reactions between glyoxylate imines **9a** or **9b** with 2,3-dihydropyrrole **7** provide the endo products in high enantioselectivity. This represents a direct route to the core tetrahydroquinoline structure of a variety of important, biologically active compounds (*21*–*23*), including martinelline (**11**, Fig. 2C), a naturally occurring nonpeptide natural product that has been identified as a bradykinin B1 and B2 receptor antagonist (*24*). The enantioselective catalytic Povarov method provides an efficient enantioselective route to this natural product and its analogs (*25*), thereby solving a longstanding synthetic challenge.

The cooperative activity of an acid and a chiral organic molecule may represent a general strategy for asymmetric catalysis (*9*, *10*), and we thus undertook a detailed experimental and computational study to elucidate the mechanism of catalysis in the Povarov reaction and the basis for the high levels of stereoselectivity induced by **1a**. Similar enantioselectivities were achieved with a variety of sulfonic acids under homogeneous conditions, and we selected the **1a**/HOTf cocatalyzed reaction between **2a** and **3** as a model for mechanistic analysis (HOTf, triflic acid, HO_3SCF_3). The reaction between **2a** (0.2 to 0.8 M) and **3** (0.4 to 1.6 M) promoted by catalytic quantities of HOTf (0.2 to 2.0 mM) alone in toluene was monitored by reaction calorimetry and ^{1}H nuclear magnetic resonance (NMR) spectroscopy (table S4). Kinetic analysis of reactions carried out at 28°C revealed a first-order dependence on [**3**] and [HOTf], and a zeroth-order dependence on imine [**2a**] (Eq. 1). These data indicate that imine **2a** undergoes quantitative protonation by HOTf under the reaction conditions, and that protioiminium triflate **2a•HOTf** represents the resting state of the achiral acid catalyst under the reaction conditions.

$$\text{Rate} = d[\mathbf{4}]/dt = k_{rac}[\text{imine}]^0[\mathbf{3}]^1[\text{HOTf}]^1_{tot} \quad (1)$$

Here, t is time and k_{rac} is the second-order rate constant for the nonenantioselective cycloaddition of **2a•HOTf** and **3**.

Consistent with this conclusion, the reaction of imine **2a** with one equivalent of HOTf resulted in the quantitative formation of protioiminium triflate **2a•HOTf** as a moisture-sensitive salt that is sparingly soluble in nonpolar solvents

(~2.0 mM in C_6D_6). The solubility of **2a•HOTf** increases by a factor of 4 in the presence of achiral urea **12** through the formation of the 1:1 complex (Fig. 3A). ^{1}H NMR chemical shifts of the formyl proton are sensitive probes of charge separation in iminium ions (*26*). We observed that the 1:1 complex of **2a•HOTf** with achiral urea **12** exhibits a 0.14 parts per million (ppm) up-field shift of the ^{1}H NMR resonance of the formyl proton of **2a•HOTf**, consistent with increased charge separation. These observations can be attributed to a hydrogen-bonding interaction between **12** and the triflate anion of **2a•HOTf** that leads to both solubilization and greater charge separation between the iminium ion and the triflate anion.

Markedly different effects are observed when **2a•HOTf** is treated with solutions of bifunctional sulfinamidourea **1a**, which increases the solubility of **2a•HOTf** by more than one order of magnitude; however, dissolution is accompanied by a 0.92-ppm down-field shift of the ^{1}H NMR resonance of the formyl proton of **2a•HOTf**, which is consistent with a less–charge-separated

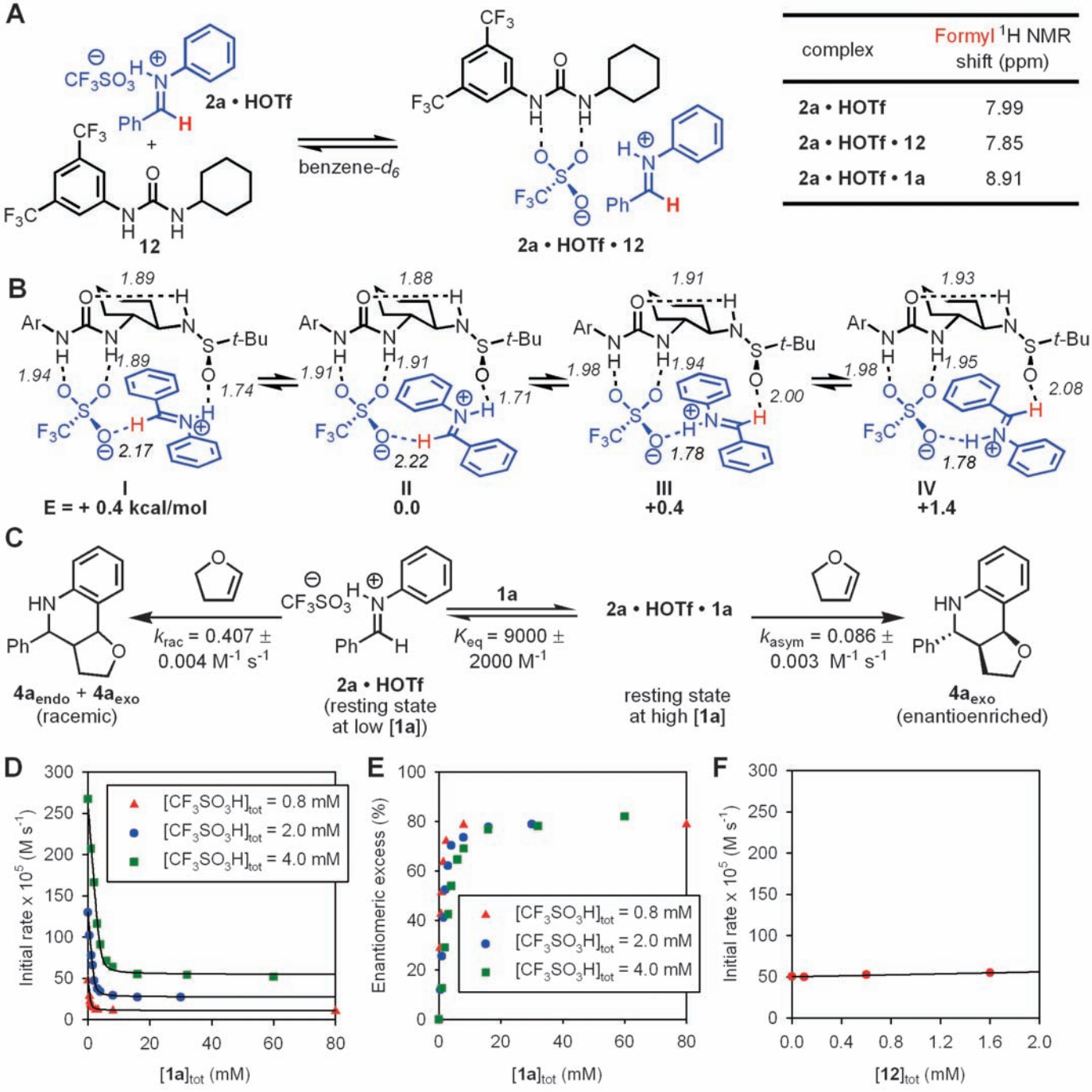

Fig. 3. (**A**) Formation of a complex between urea **12** and iminium sulfonate **2•HOTf**. ^{1}H NMR chemical shifts of the formyl proton of **2a** as free and urea-bound salts. (**B**) Geometry and energy-minimized structures of **2a•HOTf•1a** calculated at the B3LYP/6-31G(d) level of density functional theory. Ar = 3,5-$(CF_3)_2C_6H_3$. Selected bond distances are shown in angstroms. (**C**) Kinetic parameters of racemic and enantioselective Povarov reaction of **2a** and **3** cocatalyzed by **1a** and HOTf. (**D**) Plot of initial rate of the Povarov reaction versus [**1a**] at three different concentrations of HOTf. [**2a**] = 0.2 or 0.4 M, [**3**] = 1.6 M. The black curves represent least-squares fits to the rate law derived from the kinetic scheme depicted in (C). (**E**) Plot of ee of $\mathbf{4a_{exo}}$ versus [**1a**] at three different concentrations of HOTf. (**F**) Plot of initial rate of the racemic Povarov reaction cocatalyzed by achiral urea **12** and HOTf versus [**12**] with HOTf = 0.80 mM, [**2a**] = 0.2 M, [**3**] = 1.6 M.

iminium ion. Computational analysis (*27*) of the ternary **2a•HOTf•1a** complex suggests the basis for the observed effect. Four energetic minima of comparable stability were identified (Fig. 3B), with the **1a**-triflate complex acting as a dual H-bond acceptor through the triflate and sulfinamide groups, and the iminium ion acting as a dual H-bond donor through the iminium nitrogen and formyl protons (*28*).

The additional stabilizing interactions involving the catalyst-sulfinamide group and iminium ion formyl proton group have a pronounced effect on the rate of the Povarov reaction. Kinetic analysis of the reaction between **2a** and **3** that was cocatalyzed by HOTf and chiral sulfinamidourea **1a** under homogeneous conditions revealed that **1a** induces a substantial decrease in reaction rate (Fig. 3D). In contrast, the simple achiral urea **12** has a slight accelerating effect (Fig. 3F). In the presence of **1a**, the reaction rate can be expressed by a two-term rate law in which the pathway catalyzed by HOTf alone dominates at low [**1a**], and a HOTf/**1a** cocatalyzed pathway dominates at high [**1a**] (Eq. 2). A binding constant of $K = 9000 \pm 2000\ M^{-1}$ for the interaction between **1a** and **2a•HOTf** can be determined from the kinetic data (Fig. 3D and fig. S11). This relatively high value stands in sharp contrast to the much weaker binding between chiral H-bond donors and neutral substrates (*29*, *30*), but is consistent with binding constants determined between tetraalkylammonium salts and ureas and thioureas (*31*, *32*).

$$\text{Rate} = d[\mathbf{4}]/dt = k_{rac}[\text{imine•HOTf}][\mathbf{3}] + k_{asym}[\text{imine•HOTf•}\mathbf{1a}][\mathbf{3}] \quad (2)$$

Here, k_{asym} is the second-order rate constant for the enantioselective cycloaddition between **2a•HOTf•1a** and **3**.

The observation of tight binding between protio-iminium triflate **2a•HOTf** and sulfinamido urea **1a** serves to explain how high enantioselectivity is obtained during the formation of **4a**, even under conditions where the HOTf-catalyzed racemic pathway is several times more rapid than the enantioselective pathway (Fig. 3, C and E). The equilibrium constant for complex formation is sufficiently high that virtually no free iminium ion exists, and the reaction is thus channeled through the asymmetric pathway. The enantioselectivity in the formation of $\mathbf{4a}_{exo}$ is increased further to synthetically useful levels by carrying out the reaction at lower temperatures (that is, –55°C, 97% ee).

To glean insight into the basis for stereoinduction in the Povarov reaction by sulfinamidourea catalyst **1a**, we carried out a full experimental and computational analysis of the mechanism of addition of dihydrofuran **3** to the protioiminium sulfate **2•HOTf•1a**. In principle, any of several elementary steps in this process may represent the rate- and enantioselectivity-determining event (Fig. 4A, steps a to d). The absence of a primary kinetic isotope effect on the ortho hydrogens of the aniline group of **2** indicates that rearomatization (step d) is kinetically rapid (Fig. 4B). A positive Hammett correlation was obtained in the analysis of the effect of anilino substituents on the rate of reaction ($\rho = +1.96 \pm 0.06$, fig. S17). This result indicates that either the first step of a stepwise process (step a) or a concerted cycloaddition (step c) may be rate-limiting, but it is inconsistent with the cyclization step of a stepwise process (step b) representing the slow step. Definitive distinction between steps a and c is more challenging (*33*), but the kinetic isotope effect data suggest that partial rehybridization of the ortho-carbon of the aniline occurs in the rate-limiting step (*34*), and this is indicative of a concerted, albeit highly asynchronous [4+2] cycloaddition. This conclusion was supported by a computational analysis of the reaction leading to $\mathbf{4}_{exo}$, which predicts that the lowest-energy pathway involves an endothermic cycloaddition and a comparatively rapid deprotonation/rearomatization step (fig. S19).

The catalyst-bound iminium ions depicted in Fig. 3B each have one π face exposed to solvent

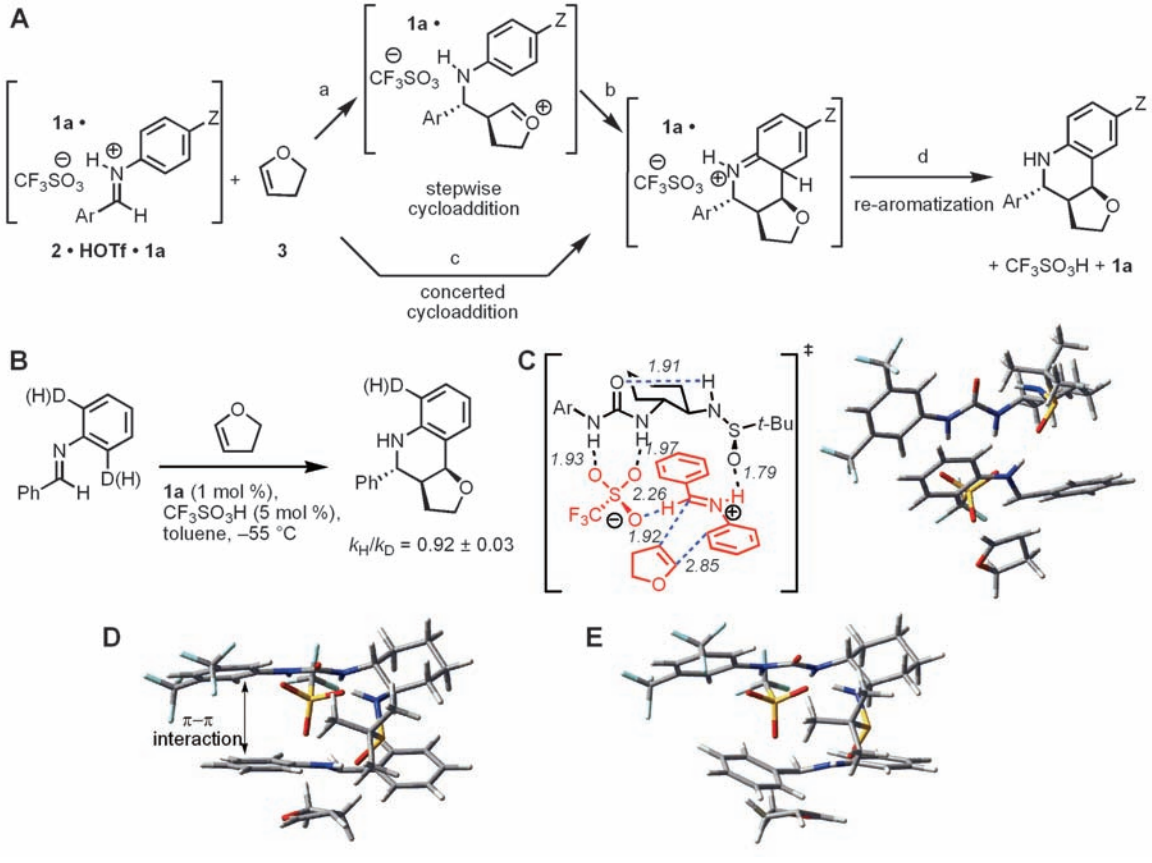

Fig. 4. (**A**) Possible mechanisms and rate-limiting steps in the asymmetric Povarov reaction. Z, an electron-donating or withdrawing substituent. (**B**) Kinetic isotope-effect experiments to distinguish between different possible rate-limiting steps. (**C**) Geometry and energy-minimized lowest-energy transition structure for cycloaddition calculated at the B3LYP/6-31G(d) level of density functional theory. Selected bond distances are shown in angstroms. Ar, 3,5-$(CF_3)_2C_6H_3$. (**D**) Alternate view of the structure in (C) highlighting the stabilizing π–π interaction between the aryl groups of the catalyst and the imimium ion undergoing cycloaddition. (**E**) Analogous view of the transition structure leading to the minor enantiomer of product. This transition structure lacks stabilizing π–π interactions and is disfavored relative to the structure in (D) by 1.3 kcal/mol in calculations using the B3LYP/6-31G(d) method, and by 3.6 to 3.9 kcal/mol using M05-2X/6-31+G(d,p) or MP2/6-31G(d) single-point calculations. See table S17 for further details.

and the other π face shielded by the catalyst, and are all expected to be energetically accessible under the reaction conditions. Computational analyses using either density functional theory or ab initio methods (Fig. 4, C to E) predict that the enantioselectivity-determining cycloaddition occurs preferentially with complex **I**, leading to the experimentally observed (*R*)-enantiomer of product $\mathbf{4a_{exo}}$. The lowest-energy cycloaddition transition structure displays iminium $N–H\cdots O_{sulfinamide}$ and formyl $C–H\cdots O_{sulfonate}$ hydrogen bonds (Fig. 4C), and is predicted to have ≥1.3-kcal/mol lower energy than alternatives arising from complexes **II** to **IV**, which is consistent with the experimental data. The basis for enantioselectivity may be ascribed to a stabilizing π–π interaction between the $(CF_3)_2$-C_6H_3N component of the catalyst and the cationic aniline moiety of the substrate. This interaction is evident in transition structures leading to the major enantiomer of $\mathbf{4a_{exo}}$ (Fig. 4D), but it is absent in transition structures leading to the minor enantiomer (Fig. 4E).

Enantioselective catalysis by **1a** of a strong Brønsted acid–catalyzed Povarov reaction thus involves tight binding to a highly reactive cationic intermediate through multiple, specific H-bonding interactions, and these noncovalent interactions are maintained in the subsequent stereodetermining cycloaddition event. One of the four energetically accessible ground-state complexes undergoes reaction with the nucleophile preferentially, illustrating the ability of bifunctional catalyst **1a** to control precisely the outcome of this reaction through noncovalent interactions alone. Given the known ability of urea and thiourea derivatives to bind a wide range of anions, the strategy demonstrated here is applicable, in principle, to cationic intermediates with a variety of counterion structures.

References and Notes

1. M. Eigen, *Angew. Chem. Int. Ed. Engl.* **3**, 1 (1964).
2. T. Akiyama, J. Itoh, K. Yokota, K. Fuchibe, *Angew. Chem. Int. Ed.* **43**, 1566 (2004).
3. D. Uraguchi, K. Sorimachi, M. Terada, *J. Am. Chem. Soc.* **126**, 11804 (2004).
4. T. Akiyama, *Chem. Rev.* **107**, 5744 (2007).
5. D. Nakashima, H. Yamamoto, *J. Am. Chem. Soc.* **128**, 9626 (2006).
6. M. Hatano, T. Maki, K. Moriyama, M. Arinobe, K. Ishihara, *J. Am. Chem. Soc.* **130**, 16858 (2008).
7. K. Ishihara, M. Kaneeda, H. Yamamoto, *J. Am. Chem. Soc.* **116**, 11179 (1994).
8. H. Yamamoto, K. Futatsugi, *Angew. Chem. Int. Ed.* **44**, 1924 (2005).
9. T. Weil, M. Kotke, C. M. Kleiner, P. R. Schreiner, *Org. Lett.* **10**, 1513 (2008).
10. R. S. Klausen, E. N. Jacobsen, *Org. Lett.* **11**, 887 (2009).
11. D. Seebach, H. A. Oei, *Angew. Chem. Int. Ed. Engl.* **14**, 634 (1975).
12. I. T. Raheem, P. S. Thiara, E. A. Peterson, E. N. Jacobsen, *J. Am. Chem. Soc.* **129**, 13404 (2007).
13. Z. Zhang, P. R. Schreiner, *Chem. Soc. Rev.* **38**, 1187 (2009).
14. A. G. Doyle, E. N. Jacobsen, *Chem. Rev.* **107**, 5713 (2007).
15. V. V. Kouznetsov, *Tetrahedron* **65**, 2721 (2009).
16. H. Ishitani, S. Kobayashi, *Tetrahedron Lett.* **37**, 7357 (1996).
17. T. Akiyama, H. Morita, K. Fuchibe, *J. Am. Chem. Soc.* **128**, 13070 (2006).
18. H. Liu, G. Dagousset, G. Masson, P. Retailleau, J. P. Zhu, *J. Am. Chem. Soc.* **131**, 4598 (2009).
19. Materials and methods are available as supporting material on *Science* Online.
20. K. L. Tan, E. N. Jacobsen, *Angew. Chem. Int. Ed.* **46**, 1315 (2007).
21. P. D. Leeson *et al.*, *J. Med. Chem.* **35**, 1954 (1992).
22. R. A. Batey, P. D. Simoncic, D. Lin, R. P. Smyj, A. J. Lough, *Chem. Commun. (Camb.)* (7): 651 (1999).
23. M. Takamura, K. Funabashi, M. Kanai, M. Shibasaki, *J. Am. Chem. Soc.* **123**, 6801 (2001).
24. K. M. Witherup *et al.*, *J. Am. Chem. Soc.* **117**, 6682 (1995).
25. C. F. Xia, L. S. Heng, D. W. Ma, *Tetrahedron Lett.* **43**, 9405 (2002).
26. H. Mayr, A. R. Ofial, E. U. Wurthwein, N. C. Aust, *J. Am. Chem. Soc.* **119**, 12727 (1997).
27. M. J. Frisch *et al.*, Gaussian 03, Revision E.01 (Gaussian, Wallingford, CT, 2004).
28. G. R. Elia, R. F. Childs, J. F. Britten, D. S. C. Yang, B. D. Santarsiero, *Can. J. Chem.* **74**, 591 (1996).
29. P. Vachal, E. N. Jacobsen, *J. Am. Chem. Soc.* **124**, 10012 (2002).
30. P. R. Schreiner, A. Wittkopp, *Org. Lett.* **4**, 217 (2002).
31. J. L. Sessler, P. A. Gale, W.-S. Cho, *Anion Receptor Chemistry* (RSC Publishing, Cambridge, UK, 2006).
32. T. R. Kelly, M. H. Kim, *J. Am. Chem. Soc.* **116**, 7072 (1994).
33. J. González, K. N. Houk, *J. Org. Chem.* **57**, 3031 (1992).
34. N. Isaacs, In: *Physical Organic Chemistry*. (Wiley, New York, 1995), pp. 296–301.

35. This work was supported by NIH (grants GM-43214 and P50 GM-69721) and by fellowship support from the Dreyfus Foundation (to H.X.), the American Chemical Society and Roche (to S.J.Z.), and the American Chemical Society through the Irving S. Sigal Postdoctoral Fellowship (to M.G.W.). We thank L. P. C. Nielsen for helpful discussions. Metrical parameters for a derivative of compound $\mathbf{4a_{exo}}$ are available free of charge from the Cambridge Crystallographic Data Centre.

Supporting Online Material

www.sciencemag.org/cgi/content/full/327/5968/986/DC1
Materials and Methods
SOM Text
Figs. S1 to S19
Tables S1 to S17
References

5 October 2009; accepted 13 January 2010
10.1126/science.1182826

100-Million-Year Dynasty of Giant Planktivorous Bony Fishes in the Mesozoic Seas

Matt Friedman,[1]* Kenshu Shimada,[2,3] Larry D. Martin,[4] Michael J. Everhart,[3] Jeff Liston,[5] Anthony Maltese,[6] Michael Triebold[6]

Large-bodied suspension feeders (planktivores), which include the most massive animals to have ever lived, are conspicuously absent from Mesozoic marine environments. The only clear representatives of this trophic guild in the Mesozoic have been an enigmatic and apparently short-lived Jurassic group of extinct pachycormid fishes. Here, we report several new examples of these giant bony fishes from Asia, Europe, and North America. These fossils provide the first detailed anatomical information on this poorly understood clade and extend its range from the lower Middle Jurassic to the end of the Cretaceous, showing that this group persisted for more than 100 million years. Modern large-bodied, planktivorous vertebrates diversified after the extinction of pachycormids at the Cretaceous-Paleogene boundary, which is consistent with an opportunistic refilling of vacated ecospace.

The largest vertebrates—fossil or living—are marine suspension feeders. Modern clades adopting this ecological strategy diversified in the Paleogene (66 to 23 million years ago) (*1*–*3*) and include baleen whales and four independent lineages of cartilaginous fishes (sharks and rays) (*4*). In striking contrast to the array of giant suspension feeders found in Cenozoic marine environments, this guild has appeared to be absent during most of the Mesozoic, an interval that is marked by the ecological ascendance of modern plankton groups (*5*, *6*). Possible candidates have been proposed (*7*, *8*), but the clearest examples of large-bodied planktivores in the Mesozoic seas have been a handful of bony fishes confined to a brief 20-million-year window during the Jurassic (Callovian-Tithonian, 165 to 145 million years ago) and known almost exclusively from European deposits (*9*–*12*). These enigmatic taxa belong to the extinct family †Pachycormidae (the dagger symbol indicates extinct groups), a stem-teleost clade that is otherwise composed of pelagic predators convergent upon tunas and billfishes (*10*). Giant †pachycormids include the largest bony fish of all time (the ~9 m †*Leedsichthys*) (*9*, *13*), but their short stratigraphic range had implied that they were an inconsequential component of

[1]Department of Earth Sciences, University of Oxford, Parks Road, Oxford OX1 3PR, UK. [2]Environmental Science Program and Department of Biological Sciences, DePaul University, 2325 North Clifton Avenue, Chicago, IL 60614, USA. [3]Sternberg Museum of Natural History, Fort Hays State University, 3000 Sternberg Drive, Hays, KS 67601, USA. [4]Natural History Museum and Biodiversity Research Center, University of Kansas, 1345 Jayhawk Boulevard, Lawrence, KS 66045, USA. [5]Division of Ecology and Evolutionary Biology, Faculty of Biomedical and Life Sciences, University of Glasgow, University Avenue, Glasgow G12 8QQ, UK. [6]Triebold Paleontology and Rocky Mountain Dinosaur Resource Center, 201 South Fairview Street, Woodland Park, CO 80863, USA.

*To whom correspondence should be addressed. E-mail: mattf@earth.ox.ac.uk